Improved Version of the Second-Order Mur Absorbing Boundary Condition Based on a Nonstandard Finite Difference Model

J. B. Cole and D. Zhu

University of Tsukuba, Japan
cole@is.tsukuba.ac.jp

***Abstract* –** It is often necessary to terminate the computational domain of an FDTD calculation with an absorbing boundary condition (ABC). The Perfectly Matched Layer (PML) is an excellent ABC, but it is complicated and costly. Typically at least 8 layers are needed to give satisfactory absorption. Thus in a 100^3 domain less than 84^3 or 59% of the grid points are usable. The second-order Mur ABC requires just 2 layers, but its absorption is inadequate for many problems. In this paper we introduce an improved version of the second-order Mur ABC based on a nonstandard finite difference (NSFD) model which has the same low computational cost but with much better absorption on a coarse grid.

Keywords: Absorbing Boundary Condition, ABC, Mur ABC, Nonstandard Finite Difference, FDTD.

I. INTRODUCTION

Unless the computational domain boundary is periodic or the fields vanish on it, an absorbing boundary condition (ABC) is needed for finite difference time domain (FDTD) calculations. An ideal ABC absorbs fields incident at all angles without reflection, and thus mimics an infinite computational domain. Except in one dimension, there is no perfect ABC. In general, the better the ABC, the more complicated and computationally costly it is. The second-order Mur ABC [1] is simple and economical, but it performs poorly at incidence angles greater than about 30° from the boundary normal. The PML [2] can, in principle, absorb fields at high incidence angles with arbitrarily low reflection, but it is complicated and costly to implement. Using a nonstandard (NS) finite difference model of the Engquist-Majda [3] one-way wave equations we derive an improved version of the Mur ABC that delivers much better absorption for the same computational cost.

II. ENGQUIST-MAJDA ONE-WAY WAVE EQUATIONS

The two-dimensional wave equation can be expressed in the form,

$$\left(\partial_t^2 - v^2\partial_x^2 - v^2\partial_y^2\right)\psi(\boldsymbol{x},t) = 0 \tag{1.1}$$

where $\boldsymbol{x} = (x, y)$ Defining $P = \sqrt{\partial_t^2 - v^2\partial_y^2}$, equation (1.1) can be factored into,

$$\left(P + v\partial_x\right)\left(P - v\partial_x\right)\psi(\boldsymbol{x},t) = 0 \tag{1.2}$$

to yield the Engquist-Majda (EM) one-way wave equations,

$$\left(P \pm v\partial_x\right)\psi(\boldsymbol{x},t) = 0\,. \tag{1.3}$$

General solutions of equation (1.3) are $\varphi_\pm(\boldsymbol{x},t) = f(\hat{\boldsymbol{k}}\bullet\boldsymbol{x} \mp vt)$, where $\hat{\boldsymbol{k}} = (\cos\theta, \sin\theta)$ and f an arbitrary function, θ is the angle $\hat{\boldsymbol{k}}$ makes with the x-axis. $P \pm v\partial_x$ absorbs waves moving in the $\pm x$-directions, respectively. On the domain $(0 \le x \le a)\times(0 \le y \le b)$, solving $\left(P \mp v\partial_x\right)\psi = 0$ at $x = 0, a$, respectively gives an ABC on the x-axis. A y-axis ABC can be similarly derived.

Since P is ill-defined, we must express it in a more suitable form. Writing $P^2 = \partial_t^2\left(1 - v^2\partial_y^2/\partial_t^2\right)$, expanding $\sqrt{P^2}$ in a Taylor series, and retaining the first two terms gives $P \cong \partial_t - \frac{1}{2}v^2\partial_y^2/\partial_t$. Inserting into equation (1.3) and multiplying by ∂_t, yields the second-order EM one-way wave equations along the x-axis,

$$\left(\partial_t^2 \pm v\partial_x\partial_t - \frac{1}{2}v^2\partial_y^2\right)\psi(\boldsymbol{x},t) = 0\,. \tag{1.4}$$

Defining $W_\pm$ to be the differential operator in equation (1.4), the annihilation error $\varepsilon_{\mathrm{EM}} = W_\pm\varphi_\pm/\varphi_\pm$ is

$$\varepsilon_{\mathrm{EM}} = v^2\frac{f''(\hat{\boldsymbol{k}}\bullet\boldsymbol{x} \mp vt)}{f(\hat{\boldsymbol{k}}\bullet\boldsymbol{x} \mp vt)}\times \left(1 - \cos\theta - \frac{1}{2}\sin^2(\theta)\right)\cdot \tag{1.5}$$

II. SECOND-ORDER MUR ABSORBING BOUNDARY

We now construct a difference equation model of equation (1.4). Taking $\Delta x = \Delta y = h$, we discretize x, y, and t in the form $x = 0, h, \cdots N_x h$, $y = 0, h, \cdots N_y h$, $t = 0, \Delta t, 2\Delta t, \cdots$. Defining the difference operators d_x, d_t', and d_x^2 by $d_x f(x) = f(x+h/2) - f(x-h/2)$, $d_t' f(t) = f(t+\Delta t) - f(t-\Delta t)$, $d_x^2 f(x) = f(x+h) + f(x-h) - 2f(x)$, finite difference expressions for the derivatives are $f'(x) \cong d_x f(x)/h$, $f'(t) \cong d_t' f(t)/2\Delta t$, and $f''(x) \cong d_x^2 f(x)/h^2$. Substituting into (1.4) yields,

$$\left(d_t^2 \pm \frac{1}{2}\frac{v\Delta t}{h} d_x d_t' - \frac{1}{2}\frac{v^2\Delta t^2}{h^2} d_y^2 \right) \psi(\mathbf{x}, t) = 0 . \quad (2.1)$$

To simplify the notation, denote the x-coordinate of the computational boundary by b, where $b = 0$ on the left, and $b = N_x h$ on the right. Let i be the x-coordinate one grid spacing inside the boundary, thus $i = b \pm h$, on the left and right respectively. The midpoint between b and i is $m = (b+i)/2$. Finally write $\psi(x, y, t) = \psi_{x,y}^t$ and $\psi(x, y, t \pm \Delta t) = \psi_{x,y}^{t\pm1}$. Evaluating (2.1) at $x = m$ using $\psi_{m,y}^t \cong \left(\psi_{b,y}^t + \psi_{i,y}^t\right)/2$, with the abbreviation $v\Delta t/h = \overline{v}$, we obtain,

$$d_t^2 \left(\psi_{b,y}^t + \psi_{i,y}^t\right) + \overline{v}\left[\left(\psi_{b,y}^{t+1} - \psi_{i,y}^{t+1}\right) - \left(\psi_{b,y}^{t-1} - \psi_{i,y}^{t-1}\right)\right] - \frac{1}{2}\overline{v}^2 d_y^2 \left(\psi_{b,y}^t + \psi_{i,y}^t\right) = 0 . \quad (2.2)$$

Henceforth, we call equation (2.2) the standard finite-difference (SFD) model of the EM equation (1.4). Equation (2.2) holds on both the left and right boundaries because $\left(\psi_{b,y}^{t\pm1} - \psi_{i,y}^{t\pm1}\right)$ has opposite signs on opposite sides. Expanding $d_t^2 \psi_{b,y}^t$ and solving for $\psi_{b,y}^{t+1}$, yields the second-order Mur ABC [4] the time-marching algorithm,

$$\psi_{b,y}^{t+1} = \psi_{b,y}^t + \left(\psi_{i,y}^t - \psi_{i,y}^{t-1}\right) + \left(\frac{1-\overline{v}}{1+\overline{v}}\right)\left[\left(\psi_{b,y}^t - \psi_{b,y}^{t-1}\right) - \left(\psi_{i,y}^{t+1} - \psi_{i,y}^t\right)\right] + \frac{1}{2}\left(\frac{\overline{v}^2}{1+\overline{v}}\right) d_y^2 \left(\psi_{b,y}^t + \psi_{i,y}^{t-1}\right) . \quad (2.3)$$

A similar expression for the $\pm y$ directions can be derived. Henceforth we call equation (2.3) the S (standard)-Mur ABC.

Let us now evaluate how well the S-Mur ABC annihilates an infinite plane wave, $\psi_\pm = e^{i(\mathbf{k}\cdot\mathbf{x} \mp \omega t)}$, with propagation vector $\mathbf{k} = k\hat{\mathbf{k}} = \left(k_x, k_y\right)$ and angular frequency $\omega = vk$. Defining the left side of equation (2.2) as $M_{\mathrm{SFD}}\psi$, where M_{SFD} is a difference operator, the annihilation error is $\varepsilon_{\mathrm{SFD}} = M_{\mathrm{SFD}}\psi_\pm / \psi_\pm$. Writing $\tilde{\varepsilon}_{\mathrm{SFD}} = \varepsilon_{\mathrm{SFD}} / 8\sin^2\left(\overline{\omega}/2\right)$, where $\omega\Delta t = \overline{\omega}$, $kh = \overline{k}$, $k_{x,y}h = \overline{k}_{x,y}$, and using the identities,

$$\psi_{b,y}^t + \psi_{i,y}^t = 2\cos\left(k_x h/2\right)\psi_{m,y}^t \quad (2.4a)$$

$$\psi_{b,y}^t - \psi_{i,y}^t = 2i\sin\left(k_x h/2\right)\psi_{m,y}^t , \quad (2.4b)$$

$$d_y^2 \psi_{x,y}^t / \psi_{x,y}^t = -4\sin^2\left(k_y h/2\right) , \quad (2.4c)$$

we find

$$\tilde{\varepsilon}_{\mathrm{SFD}}(\theta) = -\cos\left(\overline{k}_x/2\right) + \overline{v}\frac{\sin\left(\overline{k}_x/2\right)}{\tan\left(\overline{\omega}/2\right)} + \frac{1}{2}\overline{v}^2 \frac{\sin^2\left(\overline{k}_y/2\right)}{\sin^2\left(\overline{\omega}/2\right)}\cos\left(\overline{k}_x/2\right) . \quad (2.5)$$

Comparing $\varepsilon_{\mathrm{SFD}}$ with $\varepsilon_{\mathrm{EM}}$, we see that the SFD model equation (2.1) is a poor approximation to the EM equation (1.4). We now seek a better one.

III. NONSTANDARD FINITE DIFFERENCE VERSION

The SFD model of the EM equations is not the only one possible. The quantities $\overline{v}$ and $\overline{v}^2$ in equation (2.2) can be regarded as independent free parameters (u_1 and u_2^2, respectively) that can be chosen to optimize the ABC. Defining M_{NSFD} by ,

$$M_{\mathrm{NSFD}}\psi = d_t^2 \left(\psi_{b,y}^t + \psi_{i,y}^t\right) + u_1\left[\left(\psi_{b,y}^{t+1} - \psi_{i,y}^{t+1}\right) - \left(\psi_{b,y}^{t-1} - \psi_{i,y}^{t-1}\right)\right] - \frac{1}{2}u_2^2 d_y^2 \left(\psi_{b,y}^t + \psi_{i,y}^t\right) \quad (3.1)$$

we obtain a family of difference models of the EM equations, parameterized by u_1 and u_2^2,

$$M_{\mathrm{NSFD}}\psi = 0 . \quad (3.2)$$

This is an example of a nonstandard finite-difference (NSFD) model [4]. The SFD model is just the special case $u_1 = \overline{v}$, $u_2^2 = \overline{v}^2$. Let us now minimize

$\varepsilon_{\text{NSFD}} = M_{\text{NSFD}}\psi_{\pm}/\psi_{\pm}$ with respect to u_1 and u_2^2.

Writing $\tilde{\varepsilon}_{\text{NSFD}} = \varepsilon_{\text{NSFD}}/8\sin^2(\bar{\omega}/2)$, $u_1 = w_1\tan(\bar{\omega}/2)$, $u_2^2 = w_2^2\sin^2(\bar{\omega}/2)$, and making the replacements $\bar{v} \to u_1$, and $\bar{v}^2 \to u_2^2$ in equation (2.5) we obtain,

$$\tilde{\varepsilon}_{\text{NSFD}}(\theta) = -\cos(\bar{k}_x/2) + w_1\sin(\bar{k}_x/2) + \frac{1}{2}w_2^2\sin^2(\bar{k}_y/2)\cos(\bar{k}_x/2). \tag{3.3}$$

First let us require that $\tilde{\varepsilon}_{\text{NSFD}}(0) = 0$. This gives,

$$w_1 = \cot(\bar{k}/2). \tag{3.4}$$

Next inserting equation (3.4) into equation (3.3) we obtain,

$$\tilde{\varepsilon}_{\text{NSFD}}(\theta) = \delta_0(\theta) + \frac{1}{2}w_2^2\delta_2(\theta) \tag{3.5}$$

where

$$\delta_0(\theta) = -\cos(\bar{k}_x/2) + \cos(\bar{k}/2)\sin(\bar{k}_x/2), \tag{3.6a}$$

$$\delta_2(\theta) = \sin^2(\bar{k}_y/2)\cos(\bar{k}_x/2). \tag{3.6b}$$

Now requiring that $\tilde{\varepsilon}_{\text{NSFD}}(\theta_2) = 0$ yields,

$$w_2^2(\theta_2) = \frac{-2\delta_0(\theta_2)}{\delta_0(\theta_2)}. \tag{3.7}$$

The larger θ_2 the greater the absorption at high incidence angles, but the greater the reflection at intermediate angles, $0 < \theta < \theta_2$. We have examined various choices of θ_2, and conclude that the best overall choice is $\theta_2 = 45^\circ$. When radiation is incident over a wide range of large angles, however, $\theta_2 = 60^\circ$ is a reasonable compromise. We could also require that $\tilde{\varepsilon}_{\text{NSFD}}(\theta_0) = 0$ ($\theta_0 \neq 0$) and $\tilde{\varepsilon}_{\text{NSFD}}(\theta_2) = 0$ ($\theta_2 \neq \theta_0$), and simultaneously solve for w_1 and w_2^2. This choice is suitable for special applications where most of the radiation in incident on the boundary over a particular angular band. Henceforth, unless otherwise specified we take $\theta_2 = 45^\circ$.

Putting equations (3.4) and (3.7) into the expressions for u_1 and u_2^2 we have,

$$u_1 = \frac{\tan(\omega\Delta t/2)}{\tan(kh/2)} \tag{3.8a}$$

$$u_2^2(\theta_2) = -2\sin^2(\omega\Delta t/2)\frac{\delta_0(\theta_2)}{\delta_2(\theta_2)}. \tag{3.8b}$$

Inserting the simple substitutions $\bar{v} \to u_1$ and $\bar{v}^2 \to u_2^2$ into the S-Mur ABC (2.3) with the now yields the NS (nonstandard)-Mur ABC,

$$\psi_{b,y}^{t+1} = \psi_{b,y}^{t} + \left(\psi_{i,y}^{t} - \psi_{i,y}^{t-1}\right) + \left(\frac{1-u_1}{1+u_1}\right)\left[\left(\psi_{b,y}^{t} - \psi_{b,y}^{t-1}\right) - \left(\psi_{i,y}^{t+1} - \psi_{i,y}^{t}\right)\right] + \frac{1}{2}\left(\frac{u_2^2}{1+u_1}\right)d_y^2\left(\psi_{b,y}^{t} + \psi_{i,y}^{t-1}\right). \tag{3.9}$$

IV. NUMERICAL STABILITY

Consider a two-step FD algorithm of the form,

$$\psi(t+\Delta t) = a\psi(t-\Delta t) + 2b\psi(t) \tag{4.1}$$

where *a* and *b* are constants. Taking $t = \tau\Delta t$, $\tau = 0,1,2,\cdots$ and writing $\psi(t) = \psi^{\tau}$, equation (4.1) becomes,

$$\psi^{\tau+1} = a\psi^{\tau-1} + 2b\psi^{\tau}. \tag{4.2}$$

Postulating a solution to equation (4.2) of the form $\psi^{\tau} = \eta^{\tau}$, yields the equation $\eta^2 - 2b\eta - a = 0$, which has the solutions,

$$\eta_{\pm} = b \pm \sqrt{b^2 + a}. \tag{4.3}$$

The general solution of equation (4.2) is therefore,

$$\psi^{\tau} = \alpha_{+}\eta_{+}^{\tau} + \alpha_{-}\eta_{-}^{\tau} \tag{4.4}$$

where the constants $\alpha_{\pm}$ are determined by the initial values $\psi(0)$ and $\psi(\Delta t)$. Since the fields on the boundary cannot rise exponentially with time, we require that,

$$|\eta_{\pm}| \leq 1. \tag{4.5}$$

Condition (4.5) is a form of the CFL (Courant, Friedrich, Levy) [5] stability condition.

Suppose that $|\eta_+| \le 1$ and $|\eta_-| > 1$. If $\alpha_- = 0$ in equation (4.4) it might seem that $\lim_{\tau\to\infty} \psi^\tau$ is finite. In principle it is, but after a large number of iterations (N), computer round-off error gives rise to a small η_- component, and $\psi^N = a_+\eta_+^N + \delta\eta_-$. Thus ψ diverges with further iteration.

Let us now analyze the numerical stability of the NSFD model (3.2). Assuming an infinite plane wave, the spatial derivatives and averages can be expressed using equation (2.4). Equation (3.2) becomes,

$$c_x\left(\psi_{m.y}^{t+1} + \psi_{m.y}^{t-1} - 2\psi_{m.y}^{t}\right) + iu_1 s_x\left(\psi_{m.y}^{t+1} - \psi_{m.y}^{t-1}\right) + 2c_x s_y^2 u_2^2 \psi_{m.y}^{t} = 0, \tag{4.6}$$

where $s_x = \sin(k_x h/2)$, $c_x = \cos(k_x h/2)$, $s_y = \sin(k_y h/2)$. Writing $\alpha = c_x + iu_1 s_x$, and $\beta = 1 - s_y^2 u_2^2$, we can cast equation (4.6) into the form of equation (4.2) with $a = -\alpha^*/\alpha$ and $b = \beta c_x/\alpha$ in equation (4.2). The solution of equation (4.6) is thus,

$$\eta_\pm = \frac{1}{\alpha}\left[\beta c_x \pm \sqrt{\beta^2 c_x^2 - |\alpha|^2}\right]. \tag{4.7}$$

If $\beta^2 c_x^2 \le |\alpha|^2$ equation (4.7) becomes,

$$\eta_\pm = \frac{1}{\alpha}\left[\beta c_x \pm i\sqrt{|\alpha|^2 - \beta^2 c_x^2}\right] \tag{4.8}$$

whence $|\eta_\pm|^2 = 1$. On the other hand if $\beta^2 c_x^2 > |\alpha|^2$, it can be shown that either $|\eta_+| > 1$ or $|\eta_-| > 1$. The CFL condition is thus $\beta^2 c_x^2 \le |\alpha|^2$, which can be rewritten as,

$$\frac{\left(1 - s_y^2 u_2^2\right)^2}{1 + u_1^2\left(s_x^2/c_x^2\right)} \le 1. \tag{4.9}$$

Because the denominator is ≥ 1 and $s_y^2 \le 1$, equation (4.9) reduces to,

$$u_2^2(\theta_2) \le 2. \tag{4.10}$$

For the S-Mur ABC, $u_2^2 = (v\Delta t/h)^2$ and equation (4.9) gives the stability condition $v\Delta t/h \le \sqrt{2}$. For the NS-Mur ABC, putting equation (3.8) into equation (4.9) and using $\omega = kv \Rightarrow \bar{\omega} = \bar{v}\bar{k}$, the stability condition becomes,

$$-\sin^2\left(\bar{v}\bar{k}/2\right) \le \frac{\delta_2(\theta_2)}{\delta_0(\theta_2)}. \tag{4.11}$$

Since the maximum spacing between the grid points is $h\sqrt{2}$, the Nyquist sampling condition requires that we choose $\lambda/h > 2\sqrt{2} \Rightarrow 0 < \bar{k} < \pi/\sqrt{2}$. We now seek the maximum value, c, of $\bar{v} = v\Delta t/h$ such that equation (4.11) is satisfied. Numerically solving equation (4.11) gives $c = 1.31$ for $\theta_2 = 45^\circ$, and $c = 1.22$ $\theta_2 = 60^\circ$. The NS-Mur stability condition can now be expressed in the form,

$$\frac{v\Delta t}{h} \le c(\theta_2). \tag{4.12}$$

These stability constraints are looser than that of the FDTD algorithm used to compute the fields in the interior of the computational domain. In the standard (S) FDTD (Yee) algorithm, the CFL stability condition is $v\Delta t/h \le \sqrt{2}/2 \cong 0.70$, but the nonstandard (NS) FDTD algorithm [6,7] is stable for $v\Delta t/h \le 0.84$ in two dimensions. We used the NS-FDTD algorithm to calculate the electromagnetic fields in the interior of the computational domain in the results shown below.

The above analysis applies to an infinite plane wave impinging at arbitrary angle on an infinite computational boundary. A difficulty common to all ABCs is the indeterminacy of the corner points. At the corners the stability analysis is extremely difficult so it is best verified numerically. We have found that computing the ABC at the corner points with either the left-right (x-axis) ABC or the top-bottom (y-axis) ABC yields excellent stability. Some authors take the average of the left-right and top-bottom ABCs. While the resultant ABC is stable, it does not increase the absorption.

V. IMPLEMENTATION

The implementation of the ABC depends upon the details of the FDTD algorithm used to compute the electromagnetic fields, such as the placement of the electromagnetic fields on the numerical grid. For example, if the magnetic field ($\boldsymbol{H}$) is updated first in the TE mode ($H_x = H_y = E_z = 0$) with periodic FD operators, the ABC need be applied only to H_z because the electric field ($\boldsymbol{E}$) depends only on H_z. If d_x is periodic on $x = 0, h, \cdots N_x h$, then $d_x f(N_x h) = f(0) - f(N_x h - h)$, and $d_x f(0) = f(h) - f(N_x h)$.

VI. COMPARISONS AND PERFORMANCE TESTS

To test the effectiveness of our ABC we used a modification of the test described in [2] (equation (6.46), p. 258) and [8]. Expressing equation (6.46) of [2] in the space domain we have,

$$p_0(x) = \frac{1}{32}\Big[10 - 15\cos\left(\tfrac{1}{3}k_p x\right) + 6\left(\tfrac{2}{3}k_p x\right) - \cos k_p x\Big]. \quad (6.1)$$

We center the pulse at $x = 0$ by defining,

$$p(x) = p_0\left(x - \tfrac{3}{2}\lambda_p\right) \quad (6.2)$$

where $\lambda_p = 2\pi/k_p$, equation (6.2) defines a smooth pulse of half-width λ_p. To suppress periodicity we add the condition $p(x) = 0$ for $|x| > \lambda_p$. In [2] $\lambda_p = 40h/3$, but we take $\lambda_p = 2\lambda$, and use (6.2) to construct a square incident pulse envelope for a signal of wavenumber $k = 2\pi/\lambda$ as depicted in Fig. 1.

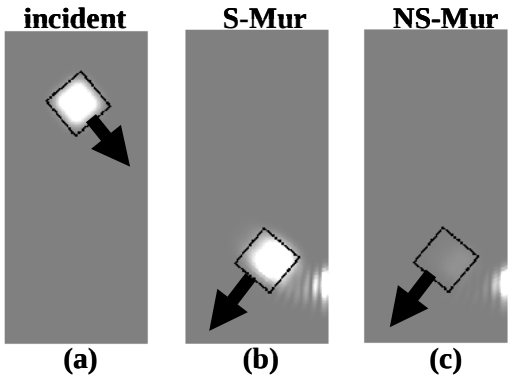

Fig. 1. (a) Incident pulse (50° from normal) reflects from the right boundary where (b) the S-Mur ABC or (c) the NS-Mur ABC is enforced.

Figure 1 depicts a typical calculation. Using the NS-FDTD algorithm, the input pulse (Fig. 1(a)) is propagated onto the right boundary, where either the S-Mur ABC (Fig. 1(b)), or the NS-Mur ABC (Fig. 1(c)) is enforced ($\theta_2 = 45^\circ$). Incident intensity I_0, is the mean intensity of the incident pulse within the box (outlined in black, Fig. 1(a)). The reflected pulse is propagated away from the boundary, and the reflected intensity (I_r), mean intensity within the box, is recorded. The intensity reflection coefficient is $r = I_r/I_0$. Note that the reflected pulse is not exactly centered within the box. Box position is computed under the assumption that the angle of reflection equals the angle of incidence, and that pulse group velocity equals phase velocity.

We also investigated the total energy absorption, by comparing total incident energy (E_0) with total reflected energy (E_r). Total energy is the local intensity summed over all grid points in the computational domain interior. The total energy reflection coefficient is $\rho = E_r/E_0$. Before reflection, the energy is concentrated about the pulse center, but afterwards some of the energy remains near the boundary and propagates along it (lower right of Figs. 1(a) and (b)). Thus r and ρ are somewhat different. For $\theta_2 = 45^\circ$ in equation (3.7) for the NS-Mur ABC, the difference is very small, but for $\theta_2 = 60^\circ$, ρ is much greater than r. For this reason we take $\theta_2 = 45^\circ$. In all that follows "NS-Mur ABC" means $\theta_2 = 45^\circ$.

Figures 2 and 3 show plots of the intensity reflection coefficient (r) as a function of incidence angle (θ) for the S-Mur, and NS-Mur ABCs. In Fig. 4 ρ is similarly plotted.

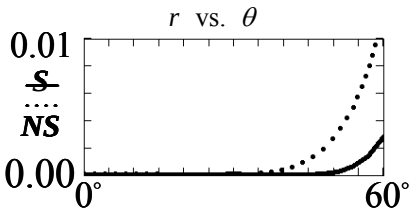

Fig. 2. Intensity reflection coefficient (r) vs. incidence angle (θ) for the S-Mur ABC (S), and NS-Mur_ABC (NS); $\lambda/h = 8$, $v\Delta t/h = 0.84$.

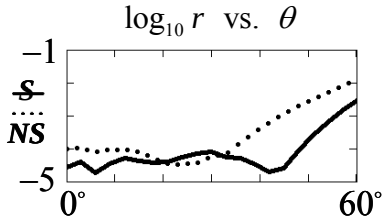

Fig. 3. Same data as Fig. 2, $\log_{10} r$ versus θ.

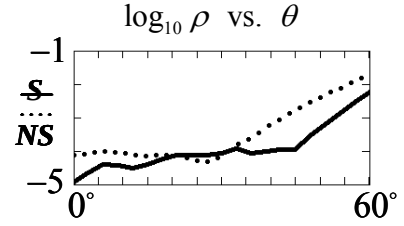

Fig. 4. Total energy reflection coefficient (ρ) vs. incidence angle (θ) for the S-Mur ABC (S), and NS-Mur_ABC (NS), $\lambda/h = 8$, $v\Delta t/h = 0.84$.

The NS-Mur ABC has the lowest values of both r and ρ over the range $0 \le \theta \le 45^\circ$, except in the narrow band $25^\circ \le \theta \le 30^\circ$, where the S-Mur ABC is slightly lower. For $\theta > 30^\circ$, S-ABC reflection rises rapidly and is always much higher than NS-ABC reflection.

We investigated the "global" energy absorption due to a pulsed point source centered in a $\lambda \times \lambda$ computational domain. Using equation (6.1) in the time domain ($k_p \to \omega_p = 2\omega_0$) to modulate a source of angular frequency ω_0, we plot the signal decay as a function of time step in Fig. 5.

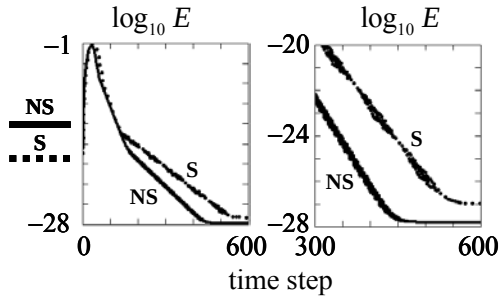

Fig. 5. Total energy (veritcal) vs. time step for the S-Mur ABC (S), and NS-Mur_ABC (NS); $\lambda/h = 8$. Right figure shows magnified scale.

As Fig. 5 shows, not only is the global energy absorption higher for the NS-Mur ABC, but also the signal decays more quickly. This faster decay is probably because the signal requires fewer "bounces" off the boundary to be absorbed.

Since the NS-Mur ABC is optimized to absorb a particular angular frequency, ω_0, it is interesting to investigate in greater detail how well it absorbs pulses. Fig. 6 depicts a normally incident pulse, and its S-Mur ABC and NS-Mur ABC intensity reflections.

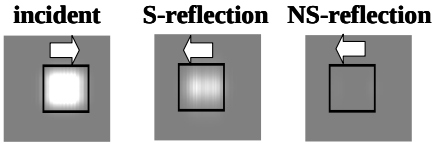

Fig. 6. Normally Incident and reflected pulses with the S-Mur and NS-Mur ABCs.

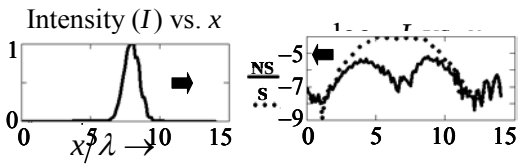

Fig. 7. Intensity profile of pulses in Fig. 6. Left: incident pulse; right: reflected pulses.

Where the pulse rises and falls $\omega \ne \omega_0$ frequency components are large but the NS-Mur ABC reflected intensity is still less than 10^{-1} that of the S-Mur ABC. In pulse center the NS-Mur ABC reflected intensity is less than 10^{-3} that the S-Mur ABC, as shown in Fig. 7.

To compute propagation in a photonic crystal consisting of vacuum holes in a dielectric substrate of refractive index n_s, we set $v\Delta t/h = c_0 = 0.84$ in the vacuum, and take $v\Delta t/h = c_0/n_s$ in the substrate. The total energy reflection (ρ) using both the S-Mur and NS-Mur ABC is little affected by the value of $v\Delta t/h$ but the intensity reflection (r) decreases somewhat for $\theta > 55^\circ$. This is, however, probably due to pulse spreading. We also examined the sensitivity of r and ρ to the value of λ/h, but found little effect.

VII. SUMMARY AND CONCLUSIONS

The NSFD version of the second-order Mur ABC is obtained with the simple replacements $\overline{v} \to u_1$, and $\overline{v}^2 \to u_2^2$. We found that the best ABC for general use is the choice $\theta_2 = 45^\circ$ in equation (3.7). Existing computer codes can be easily modified to give much better absorption for the same computational cost. Although the NS-Mur ABC is optimized for monochromatic radiation, it also absorbs moderately broad pulses effectively. The data of Figs. 2 to 5 are taken with bandwidth $\Delta\omega_0 \sim \omega_0/4$ about the central frequency, ω_0. The performance of the S-Mur ABC is also frequency dependent, and its performance deteriorates as λ/h decreases. On the other hand the NS-Mur ABC is optimized to grid spacing, and does well on a coarse grid. As Figs. 2-5 show, both the S-Mur ABC and NS-Mur ABC give low reflection up to incidence angles (θ) of about 30°, but the NS-Mur ABC is much better than the S-Mur ABC for $\theta > 30^\circ$.

The NS-Mur ABC is still fundamentally a second-order ABC. For wide-band absorption at high incidence angles a more sophisticated ABC, such as PML, must be used with its concomitant complexity and high computational cost.

This work greatly expands the utility of the simple, low-cost second-order Mur ABC. The foregoing developments have been extended to three dimensions. In three dimensions where there are line corners and point corners, special care must be taken to correctly join the Mur ABC with the FDTD algorithm.

REFERENCES

[1] G. Mur, "Absorbing boundary conditions for the finite-difference approximation of the time domain electromagnetic field equations," *IEEE Transactions on Electromagnetic Compatibility*, vol. 23, pp. 377-382, 1981.

[2] A. Taflove and S. C. Hagness, "Computational electrodynamics: the finite-difference time-domain method. norwood," *Artech House, Inc., Norwood, MA,* 2000.

[3] B. Engquist and A. Majda, "Absorbing boundary conditions for the numerical simulation of waves," *Mathematics of Computation,* vol. 31, pp. 629-651, 1977.

[4] R. E. Mickens, "Nonstandard finite difference models of differential equations," *World Scientific, Singapore*, 1994.

[5] S. K. Godunov, "Difference Schemes," North-Holland, Amsterdam, 1987.

[6] J. B. Cole, "High accuracy Yee algorithm based on nonstandard finite differences: new developments and verifications", *IEEE Trans. Antennas and Propagation,* vol. 50, no. 9, pp. 1185-1191, Sept. 2002.

[7] J. B. Cole, "High accuracy nonstandard finite-difference time-domain algorithms for computational electromagnetics: applications to optics and photonics," Chapter 4, pp. 89-109 in *Advances in the Applications of Nonstandard Finite Difference Schemes*, R. E. Mickens, ed., Scientific, Singapore, 2005.

[8] T. G. Moore, J. G. Blaschak, A. Taflove, and G. A. Kriegsmann, "Theory and application of radiation boundary operators," *IEEE Trans. Antennas and Propagation*, vol. 36, pp. 1797-1812, 1988.